Minimizing thermal residual stresses in ceramic matrix composites by using DE and ANN-based response surface method

TAO YOU, QIMAN WU, YINGJIE XU[a, *]
Institute of Computer Testing, Control and Simulation, School of Computer Science, Northwestern Polytechnical University, Xi'an, 710072, China
[a]*Engineering Simulation and Aerospace Computing, Key Laboratory of Contemporary Design & Integrated Manufacturing Technology, Northwestern Polytechnical University, Xi'an, 710072, China*

The thermal residual stresses (TRS) induced in ceramic matrix composites (CMCs) with multi-layered interphases when cooling down from the processing temperature, have a significant influence on the mechanical behavior and lifetime of CMCs. The objective of this work is to minimize the TRS of the unidirectional CMCs with multi-layered interphases by controlling the interphases thicknesses. A hybrid strategy incorporating finite element computation, artificial neural network (ANN)-based response surface method (RSM) and differential evolution (DE) algorithm is proposed to predict the TRS of CMCs. The finite element method is adopted to calculate the TRS distribution within CMCs and the ANN-based RSM (ANNRSM) is employed to approximate the non-linear relationship between the design parameters and the TRS of the designed CMCs. The well-trained ANNRSM is finally used to find the minimum TRS. The results show the proposed methodology could estimate the TRS of different design solutions and identify the best one.

1. Introduction

Ceramic matrix composites (CMCs) with continuous fibre reinforcement exhibit attractive properties for thermal-structural applications, including low density, high strength and non-brittle mechanical behavior. This last property is controlled by the presence of an interphase between the fibres and the matrix [1, 2]. The most commonly used interphase materials are pyrocarbon (PyC) and boron nitride (BN), which allow fibre debonding and crack deflection with energy dissipation. However, both of them are not stable under oxidizing conditions at high temperatures. Recently, CMCs with multi-layered interphases that have both oxidation resistance and high strength have been developed [3, 4]. The multi-layered interphases consist in alternating sub-layers of two different materials, for instance, PyC and anti-oxidative silicon carbide (SiC) associated in a sequence of n PyC/SiC layers (denoted as (PyC/SiC)n) [5, 6].

In CMCs with multi-layered interphases, thermal residual stresses (TRS) are often generated upon cooling from processing to room temperatures due to extensive mismatch of the coefficients of thermal expansion (CTE) between the constituents (fibre, interphase and matrix). The distribution of TRS, resulting in the cracks and

separations in the matrix and interphases, has a significant influence on the mechanical behavior and lifetime of CMCs. Finite element method [7-9] have been widely used for numerical computation of TRS in CMCs. However, efforts to optimize the distribution of TRS in the multi-layered interphases and matrix of CMCs have not been made yet systematically. The multi-layered interphases are usually obtained by using the chemical vapor infiltration (CVI) process [10, 11]. During the CVI process, the thicknesses of layers are controllable. To achieve an excellent thermal-mechanical performance of CMCs, it is necessary to analyze and design the thicknesses of the multi-layered interphases for an optimized TRS distribution. Motivated by this situation, the present paper is directed at minimizing the TRS of CMCs with multi-layered interphases based on finite element computation.

The critical issue in minimizing the TRS is to find the optimized combination of multi-layered interphases thicknesses. A subtle change of any interphase will constitute a new design scenario and a new finite element simulation is needed to explore its behaviours and performance. Due to the complex multi-layer microstructure and large heterogeneity of multi-phase materials, a detailed finite element model usually involves

ten thousands of elements and the computational cost is quite high. It is not pragmatic to find the optimal solution through one-by-one simulation. Even with the combination of FEM simulation and other soft computing technology, it cannot easily find the best design as it costs long time to conduct all the simulation for any given point in the design space.

As a remedy for suppressing the CPU time increase, the approximation method is widely adopted. The representative ones are the response surface method (RSM) [13, 14] and the employment of artificial neural network (ANN) [12]. With the RSM, a closed-form limit state surface is constructed artificially using polynomial regression. However, these methods become computationally impractical for problems involving a large number of random variables and non-linear limit state functions, particularly when statistically dependent random variables are involved. Neural networks have the advantage of their flexibility to adapt to more complex limit state functions that might not be represented well by means of a low order polynomial, so ANN-based RSM (ANNRSM) is more efficient and accurate than the conventional RSM [13, 14].

It is well known that direct training of ANN usually falls into local optimum. In order to overcome the defects of ANN algorithm, many hybrid training algorithms which combines evolution algorithms (EAs) and ANN are presented to reduce the forecast error and improve the accuracy of the model. After lots of efforts in improving, the more effective EAs are genetic algorithm (GA) [15, 16] and differential evolution (DE) [17] algorithm so far.

DE, with the advantage of powerful and effective global optimizer in the continuous search domain, is not only astonishingly simple but also performs extremely well in a wide variety of test problems. The most important advantages are that the number of preset parameters in DE algorithm is much less than other algorithms. Moreover, compared to GA, these preset parameters are more accurate and not obtained by trail-and-error in advance.

In this research, a framework on the integrating finite element computation, ANNRSM and DE algorithm is proposed to find the optimal thicknesses of the multi-layered interphases for minimum TRS. Unidirectional CMCs with multi-layered (PyC/SiC)$_n$ interphases are concerned in the present work. The methodology utilizing the finite element method to calculate the TRS distribution within CMCs and employing the ANNRSM to approximate the non-linear relationship between the design parameters and the TRS of the designed CMCs is developed. To illustrate the detailed procedure and processes, a case study is used to implement the developed methodology. The results show the proposed methodology could effectively estimate the TRS of different design solutions and identify the best one.

2. Finite element analysis of TRS
2.1. Finite element model

The architectures of unidirectional CMCs consist of arranged fibres. The components of the multi-layered (PyC/SiC)$_n$ interphases and the SiC matrix are infiltrated within the porous fibre preforms, according to the CVI process.

In the present study, square fibre arrays are used to model the unidirectional CMCs. Four layers of interphases are distributed around the fibres. Fig. 1 shows the transverse cross-section of the CMCs. In the longitudinal direction, the fibre axes have been assumed to be parallel and of equal lengths.
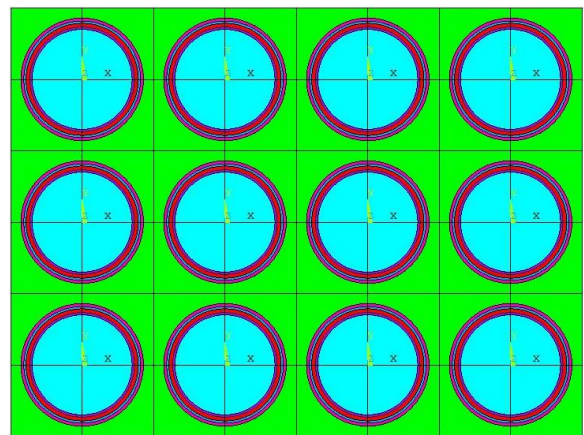
Fig. 1. Transverse cross-section of the CMCs with four layers of interphases.

The unit cell of composite (as seen in Fig. 2) is used in the present finite element analysis. Characteristic geometric parameters of the unit cell model are given: ϕ^f is fibre diameter, $d_1 \sim d_4$ are thicknesses of the interphase layers, d_5 is the thickness of the matrix layer.
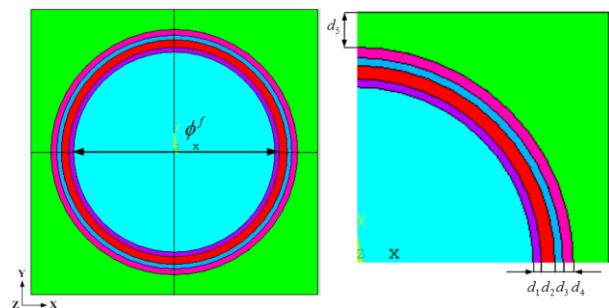
Fig. 2. Geometrical model of the unit cell.

The unit cell model is meshed using the 3D twenty-node, thermal-structural coupled element (SOLID 96) of ANSYS finite element software [21], as depicted in Fig. 3. The number of elements and nodes is 3,840 and 3,986, respectively.
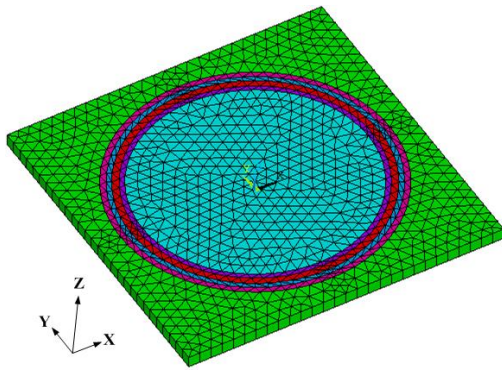
Fig. 3. Finite element model of the unit cell.

The analytical model is assumed as a perfect elastic body without plastic deformation. The structural and thermal boundary conditions are given as follows:

(1) Nodes on the boundary surfaces are free to move but have to remain planar in a parallel way to preserve the compatibility with adjacent cells.

(2) The initial stresses of all nodes are assumed as zero at the sintering temperature, and TRS generated in the succeeded cooling process.

(3) The model is assumed to cool from sintering temperature to room temperature, with a uniform temperature field. In practice, temperature of the model is decreased by ΔT and ANSYS finite element software is used to calculate the TRS in the model.

2.2. Numerical validation

Due to the complexity of the CVI fabrication process of multi-layered interphases, most of the available experimental results and numerical values evaluated by other numerical methods in the literatures are focused on the CMCs with single-layered interphase. Hence, in this section, numerical tests are dealt with to evaluate TRS of CMCs with single-layered interphase. These results are compared with experimental data and other available numerical results to show the validity of the model.

A unidirectional carbon fibre reinforced SiC ceramic matrix composite with single-layered molybdenum disiticide (MoSi$_2$) interphase (C/MoSi$_2$/SiC) is firstly studied. Residual axial and hoop thermal stresses in C/MoSi$_2$/SiC composites fabricated with 8 μm T300 carbon fibre, have been measured experimentally [7]. Fig. 4 shows the finite element model of the unit cell of C/MoSi$_2$/SiC composite with a 1/2.5 interphase/matrix thickness (μm). Similar finite element models are created for other interphase/matrix thicknesses.
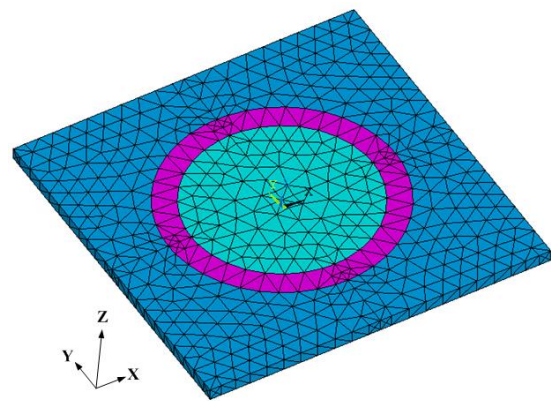
Fig. 4. Finite element model of the unit cell for C/MoSi2/SiC composite.

Material properties of the constituents are taken from reference [7] and are given in Table 1.

Table 1. Properties of the constituents.

Constituents	Elastic moduli (GPa)				Poisson ratio		CTEs ($10^{-6}/°C$)	
	E_{XX}	E_{ZZ}	G_{XY}	G_{YZ}	v_{XY}	v_{YZ}	α_{XX}	α_{ZZ}
Carbon fiber	22	220	7.75	4.8	0.4	0.12	27	0
SiC fiber	200	200	80	80	0.12	0.12	3	3
MoSi$_2$interphase	310	310	124	124	0.25	0.25	8.4	8.4
PyC interphase	12	30	4.3	2	0.4	0.12	28	2
SiC matrix	350	350	145.8	145.8	0.2	0.2	4.6	4.6

Two thermal loading states are prescribed. The unit cell is assumed initially at a uniform temperature of 1000°C (state 1). Then in state 2, the temperature is uniformly set to 0°C.

Table 2 lists the average values of the numerically obtained TRS against experimental results in reference [7]. It can be seen that the numerical results are globally in agreement with the experimental ones.

3. Case description

In this paper, a interphase thicknesses design optimization of a unidirectional SiC fiber reinforced SiC ceramic matrix composite with six layers of (PyC/SiC) interphases (SiC/(PyC/SiC)$_6$/SiC) is presented. Our goal is to obtain optimal interphases which minimize the maximum TRS in the multi-layered interphases and matrix generated upon cooling from processing (1000°C) to room

(25°C) temperatures. The diameter of the SiC fiber is 10 μm and the thickness of the SiC matrix layer is 2 μm .

Table 2. Comparison of numerical results with experimental ones.

Interphase/Matrix thickness (μm)		Axial stresses (MPa)		Hoop stresses (MPa)	
		Interphase	Matrix	Interphase	Matrix
0.3/2.1	Numerical analysis	1287	158	162	-910
	Experimental results	1190	140	230	-740
1/2.1	Numerical analysis	935	127	146	-903
	Experimental results	820	140	180	-670
0.3/2.5	Numerical analysis	1610	109	1548	232
	Experimental results	1490	120	1420	210
1/2.5	Numerical analysis	1026	87	1603	215
	Experimental results	890	120	1430	190

Usually, the layers thicknesses should be regular values without many decimal places for reducing the complexity of the CVI fabrication process. In addition, the lower bounds of thicknesses of material layers should be bigger than 0.1 μm for oxidation resistance considerations [20]. Therefore, in this study five levels are defined for each parameter as following:

$d_i = \{0.3,\ 0.4,\ 0.5,\ 0.6,\ 0.7\}\ \mu m,\ i = 1, 2, ..., 6$

In this study, the training cases are generated by finite element simulations. It can be known that large-scale computations would be involved if all the five levels of every parameter are studied (15625 combinations would be generated). Therefore, the orthogonal array is employed, which uses small amount of simulations to find out the relationship between the parameters and TRS. Here L25 orthogonal array is adopted as reference to select the combinations as training cases for the ANNRSM. There are 25 design combinations in the selected L25 orthogonal array. All the parameter combinations of the training case and the corresponding simulation results are shown in Table 3.

Table 3. Detail design combinations and corresponding results of the training cases.

Design configurations							Results		
Parameter	d_1 μm	d_2 μm	d_3 μm	d_4 μm	d_5 μm	d_6 μm	*axial TRS* GPa	*Hoop TRS* GPa	*radial TRS* GPa
Case 1	0.3	0.3	0.3	0.3	0.3	0.3	-0.039636	-0.026294	0.123096
Case 2	0.3	0.4	0.4	0.4	0.4	0.4	-0.033060	-0.026341	0.112759
Case 3	0.3	0.5	0.5	0.5	0.5	0.5	-0.029238	-0.026684	0.105307
Case 4	0.3	0.6	0.6	0.6	0.6	0.6	-0.026033	-0.027173	0.097569
Case 5	0.3	0.7	0.7	0.7	0.7	0.7	-0.023591	-0.027765	0.090743
Case 6	0.4	0.3	0.4	0.5	0.6	0.7	-0.031172	-0.024171	0.104114
Case 7	0.4	0.4	0.5	0.6	0.7	0.3	-0.025626	-0.024168	0.107663
Case 8	0.4	0.5	0.6	0.7	0.3	0.4	-0.025302	-0.025618	0.100193
Case 9	0.4	0.6	0.7	0.3	0.4	0.5	-0.028522	-0.025037	0.104094
Case 10	0.4	0.7	0.3	0.4	0.5	0.6	-0.029674	-0.027757	0.094277
Case 11	0.5	0.3	0.4	0.5	0.6	0.7	-0.027467	-0.023432	0.100099
Case 12	0.5	0.4	0.5	0.6	0.7	0.3	-0.030262	-0.022569	0.104253
Case 13	0.5	0.5	0.6	0.7	0.3	0.4	-0.025074	-0.022776	0.106754
Case 14	0.5	0.6	0.7	0.3	0.4	0.5	-0.026038	-0.025420	0.096499
Case 15	0.5	0.7	0.3	0.4	0.5	0.6	-0.025704	-0.026673	0.089752
Case 16	0.6	0.3	0.4	0.5	0.6	0.7	-0.026978	-0.020556	0.107419
Case 17	0.6	0.4	0.5	0.6	0.7	0.3	-0.026522	-0.022136	0.099257
Case 18	0.6	0.5	0.6	0.7	0.3	0.4	-0.027906	-0.024893	0.088810
Case 19	0.6	0.6	0.7	0.3	0.4	0.5	-0.022182	-0.024130	0.092645
Case 20	0.6	0.7	0.3	0.4	0.5	0.6	-0.025217	-0.023764	0.096673
Case 21	0.7	0.3	0.4	0.5	0.6	0.7	-0.023927	-0.020283	0.102528
Case 22	0.7	0.4	0.5	0.6	0.7	0.3	-0.024678	-0.023036	0.091350
Case 23	0.7	0.5	0.6	0.7	0.3	0.4	-0.027107	-0.021965	0.096506
Case 24	0.7	0.6	0.7	0.3	0.4	0.5	-0.026689	-0.023301	0.089235
Case 25	0.7	0.7	0.3	0.4	0.5	0.6	-0.022525	-0.023186	0.092276

4. Hybrid strategy based on ANNRSM and DE

The hybrid strategy defined using ANNRSM and DE approaches consists in relating the generation parameters to the multi-layered interphases thicknesses and maximum TRS ($d_1, d_2, d_3, d_4, d_5, d_6, TRS_a, TRS_h, TRS_r$). Fig. 5 shows the flowchart related to the strategy. ANNRSM learns the causal relationships from the dataset in Section 3 by a training procedure based on the DE technique, which optimizes internal parameters for ANNRSM.
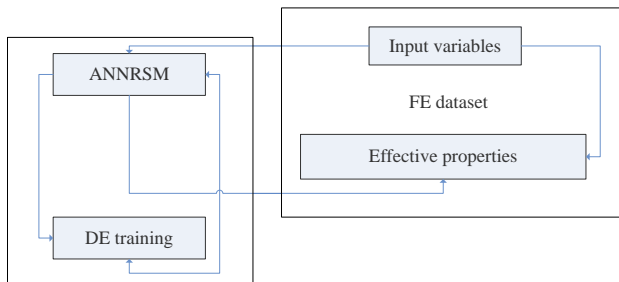
Fig. 5. Flowchart of the hybrid strategy based on ANNRSM/DE scheme.

Here, we get the neuron number (N') in the hidden layer of ANNRSM by an Extreme learning machine (ELM) method [18]. Unlike BP method, ELM for single-hidden layer feedforward neural networks (SLFNs) chooses hidden neuron number and analytically determines the output weights of SLFNs non-iteratively. This algorithm tends to provide good generalization performance at extremely fast learning speed.

SLFNs with at most N hidden nodes and with almost any nonlinear activation function can exactly learn N distinct observations. So repeat ELM by $N' \in [1, N]$, $N = 25$, according to the number of training cases in this case, we can find the best $N' = 14$. Then an ANNRSM is built to relate the input to the output parameters as illustrated in Fig. 6. Each neuron in the structure is defined using three quantities: an input, an output and a transfer function. The transfer function is a sigmoid function which is adequate for continuous variable processing [19]. W_{ij} and W_{jk} are the weight matrix representing all possible connections between the neuron outputs, hidden layer and the neuron inputs indexed by k ($k = 1, 2, 3$), j ($j = 1, 2, ..., 14$) and i ($i = 1, 2, ..., 6$).
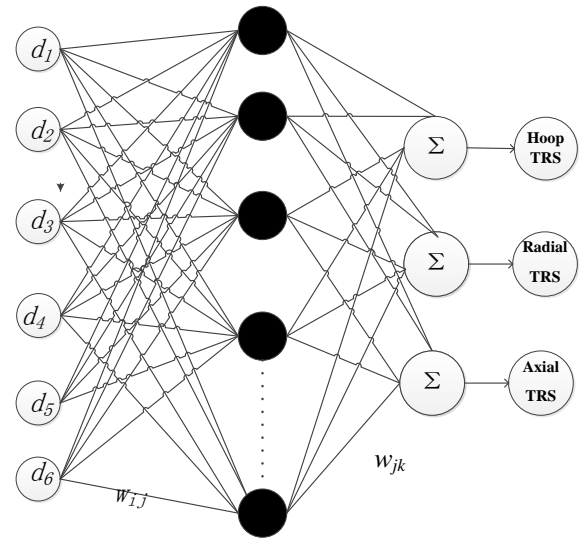
Fig. 6. Sketch of the ANNRSM used in this study.

The flow diagram of the ANNRSM in the training phase is shown in Fig. 7 and the design steps are stated as the following.

Step 1: Set the general number G=0, and randomly initialized a population with q individuals. x_i^G, as an individual, stands for the weights of ANNRSM. Then the initial population can be set by prescribing minimum and maximum bound values, $x_{k_{max}}$ and $x_{k_{min}}$.

Step 2: Each individual can be set into ANNRSM estimator to get each fitness function.

Step 3: If the offspring is not produced yet, the mutation phase will be executed. Therefore, the mutation vector will be produced in the mutation phase from each individual.

Step 4: The offspring can be chosen between parent and mutation vector via crossover operation and then go to selection phase.

Step 5: In the selection phase, the offspring vector will be compared with parent vector x_i^G by fitness function, and the better one will be selected and survived to next generation.

Step 6: After the new individual x_i^{G+1} is generated completely, it will be compared with the best-so-far individual x_{best} by the fitness function and also the better one may become the new best-so-far individual.

Step 7: If the individuals in current generation are not executed yet, then go to step 2. If all of the individuals in current generation are executed, it will enter to next generation and go to step 2.

Step 8: When the training phase is finished, the best estimated parameters can be obtained and set into ANNRSM for ANN training phase.
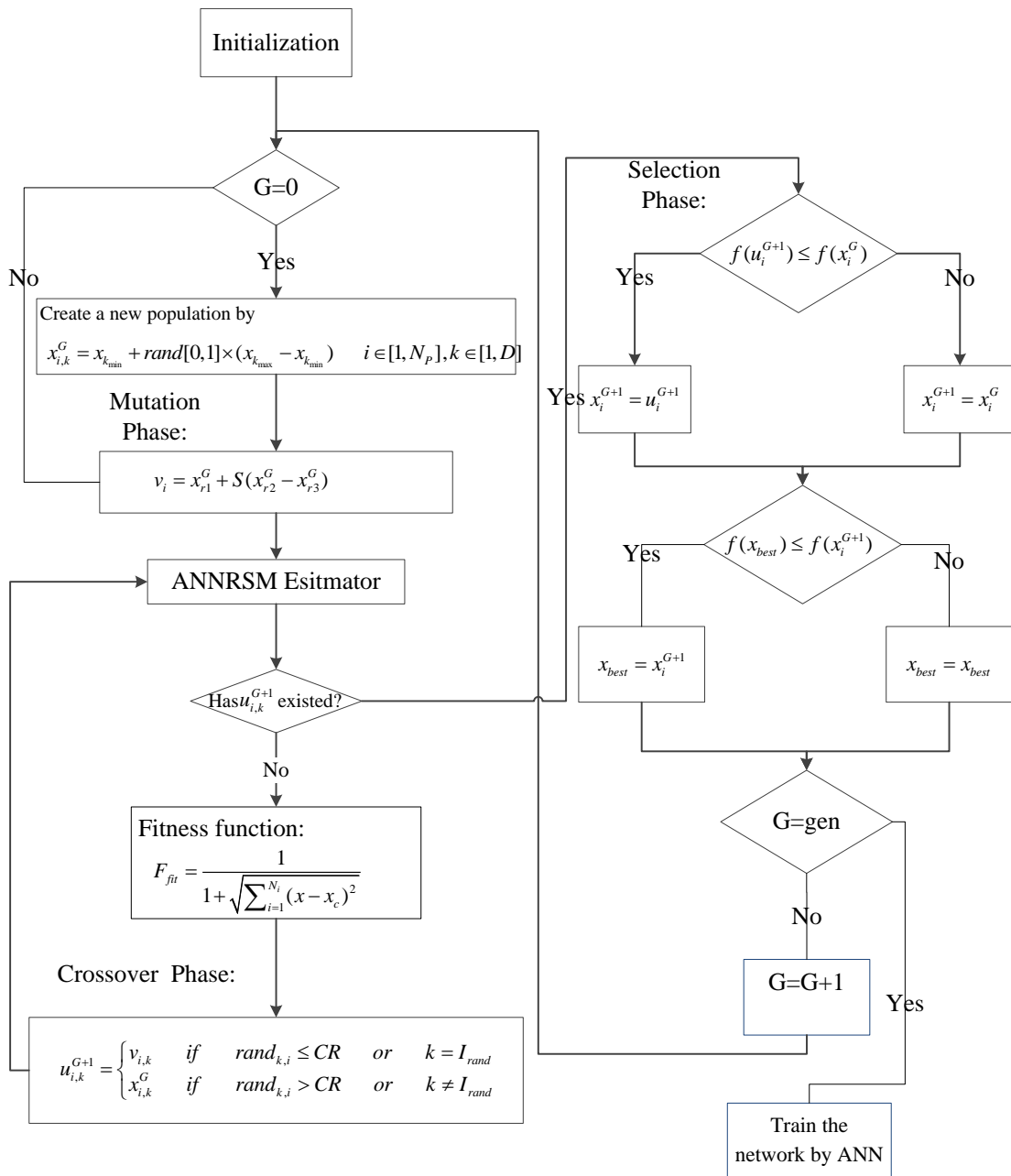
Fig. 7. The flow diagram for the training phase.

5. Results and discussion

5.1 ANNRSM training

Fig. 8 illustrates the evolution of the DE criterion (average training error sum of square curve and fitness curve) as function of the number of generations. For convergence purposes, the DE population size is 100. The number of generations is evaluated after several runs to 500 generations. The crossover and mutation operators are respectively equal to 0.6 and 0.5. In Fig. 8, the optimal solution is obtained at the 300th generation, while best,

worst and the average solutions (red, green and blue) are similar at the convergence point). In our case, one training process as that shown in Fig. 8 takes 5 min.
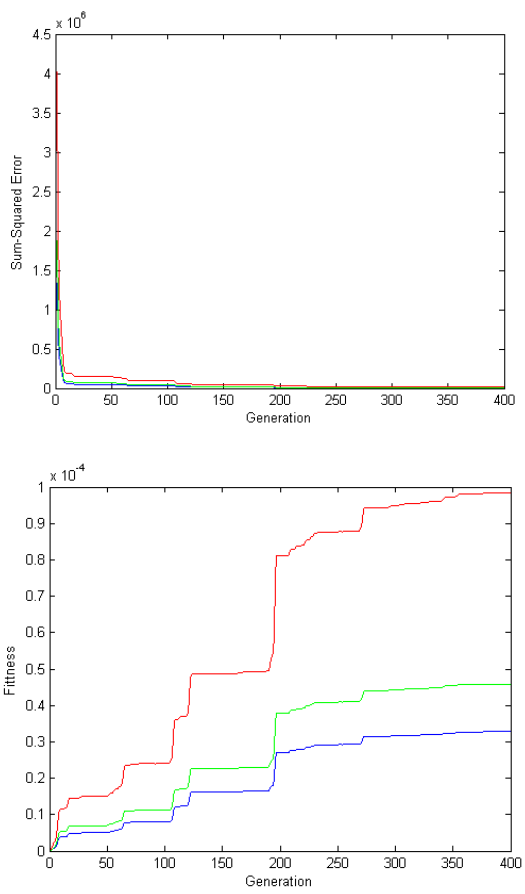
Fig. 8. Error sum of square curve and fitness curve of DE.

Fig. 9 shows a typical ANN training process monitored using the average training errors. Note that the fluctuations are significantly reduced beyond 20 iterations. The residual value after the completion of the process is less than 0.001%. So far, we get a well-trained ANNRSM.
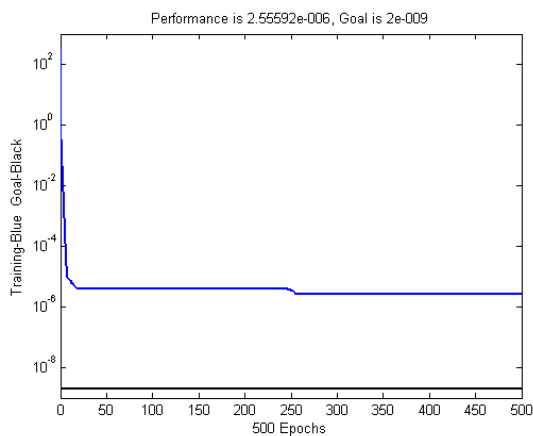
Fig. 9. Training error curve of ANNRSM.

5.2 Estimation of the TRS

In order to demonstrate the ANNRSM's ability to

generalize the training data, the ANN RSM's direct output method was used to estimate the TRS of the input parameters combination (DE and ANN training are not operating here). The FEM's and ANNRSM' results with varying the level of only one parameter are compared. Figs. 10-15 show the comparison of the FEM's and ANN-based RSM' results about the axial TRS, hoop TRS, radial RTS (6 parameters with 5 levels) respectively. The result shows the ANNRSM's prediction give a satisfactory agreement with the FEM's result.
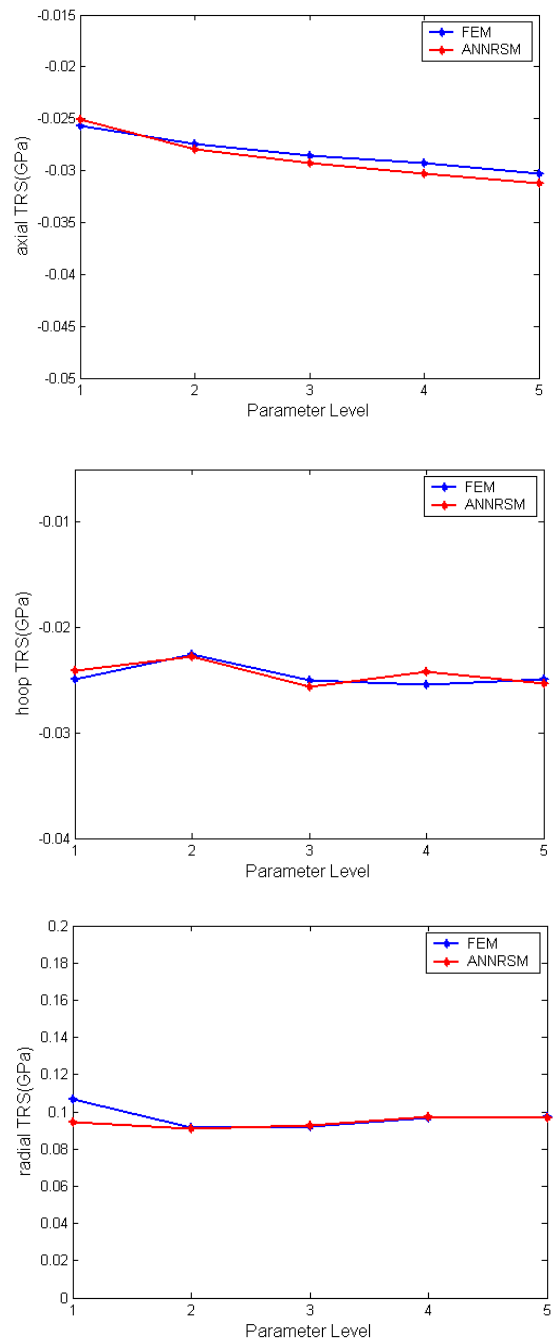
Fig. 10. Comparison of FEM's and ANNRSM's results with different level of d_1.
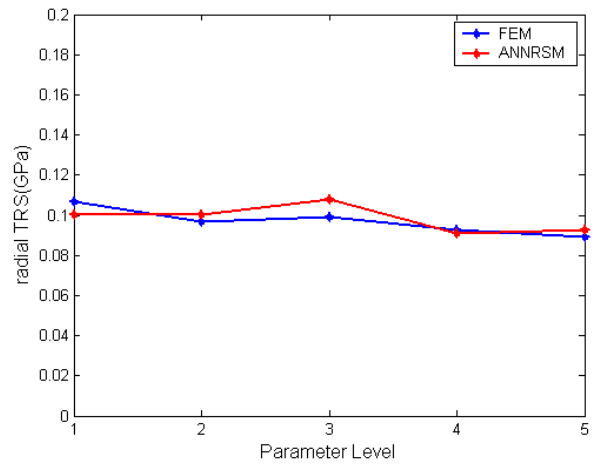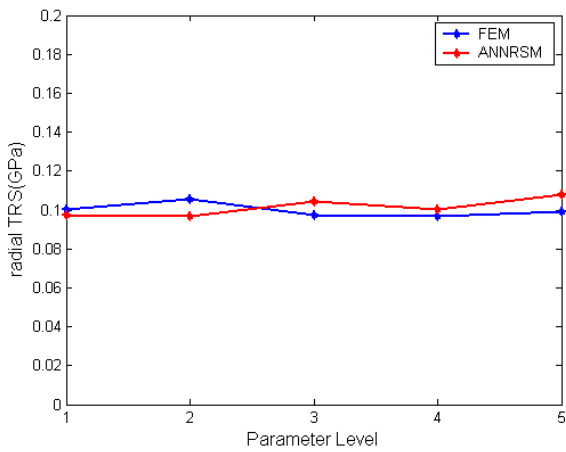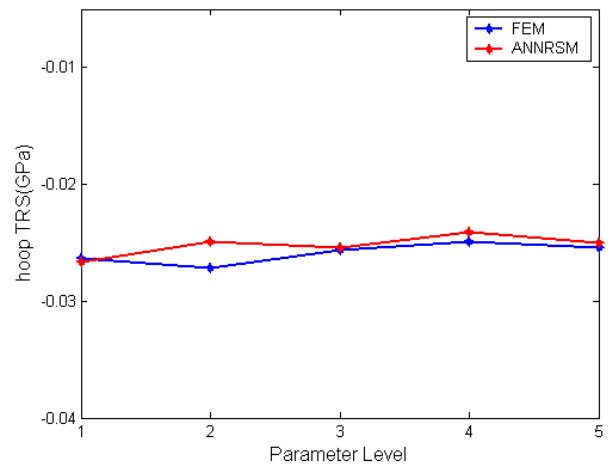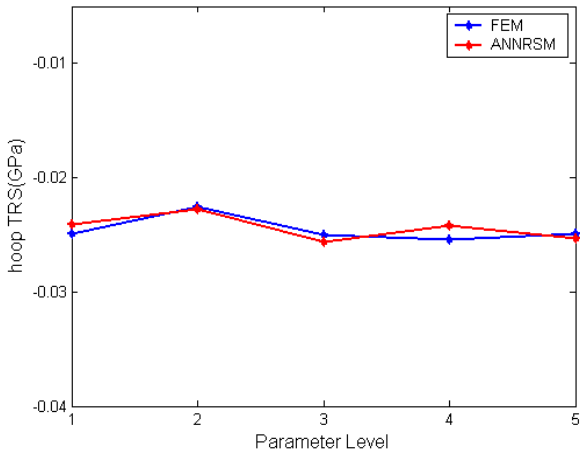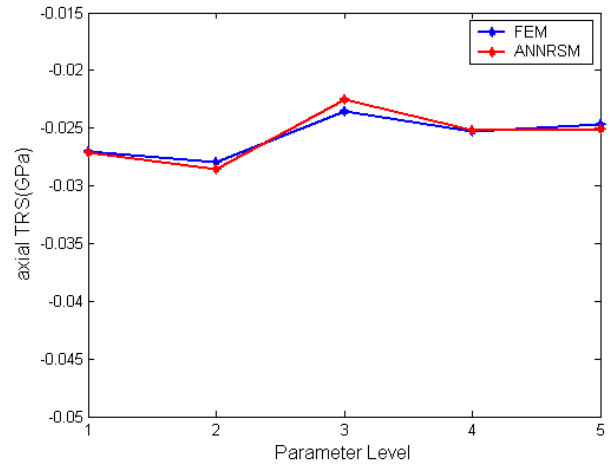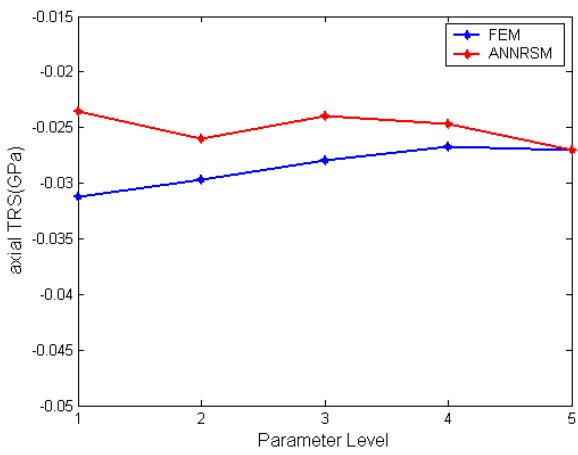
Fig. 11. Comparison of FEM's and ANNRSM's results with different level of d_2.

Fig. 12. Comparison of FEM's and ANNRSM's results with different level of d_3.
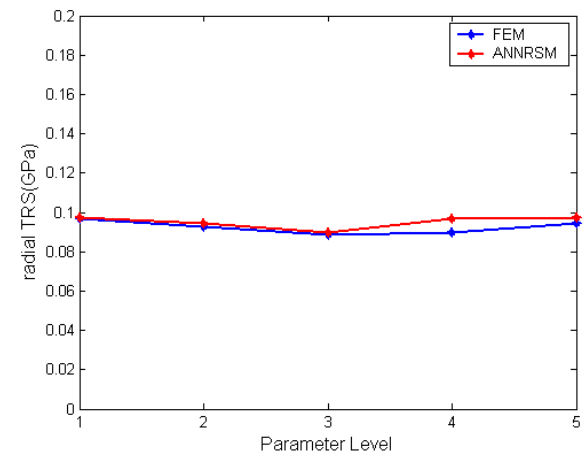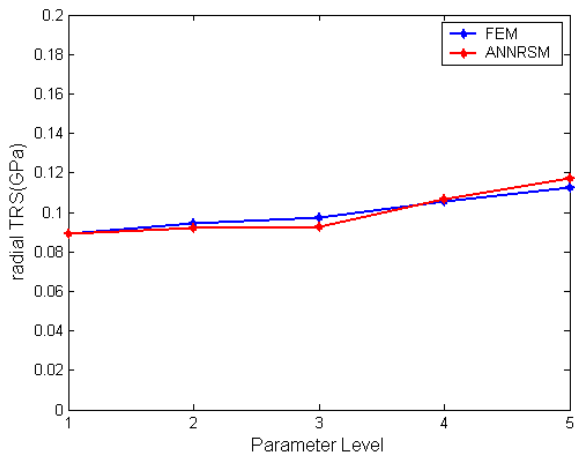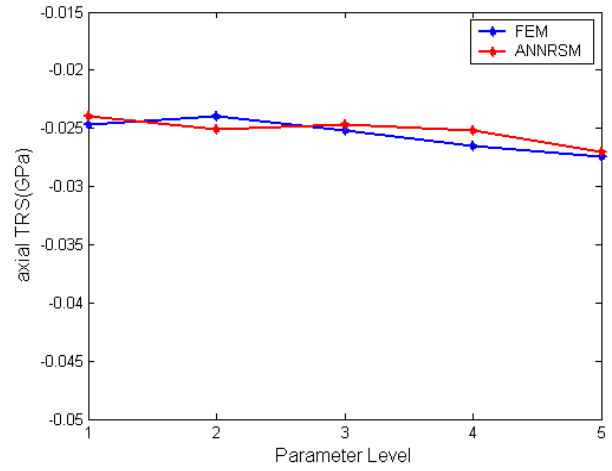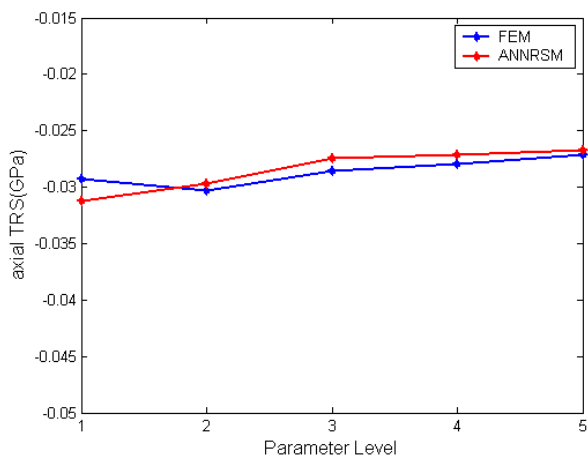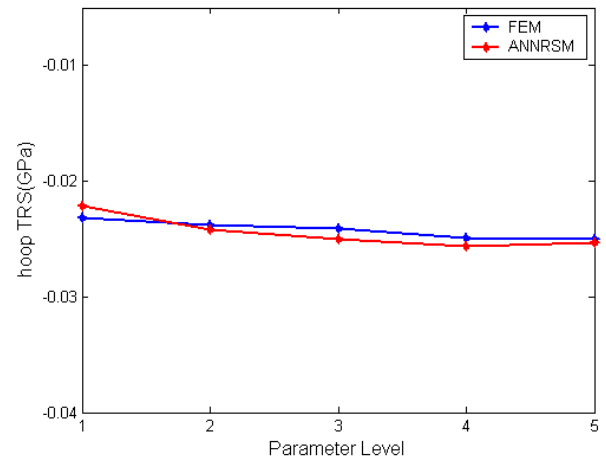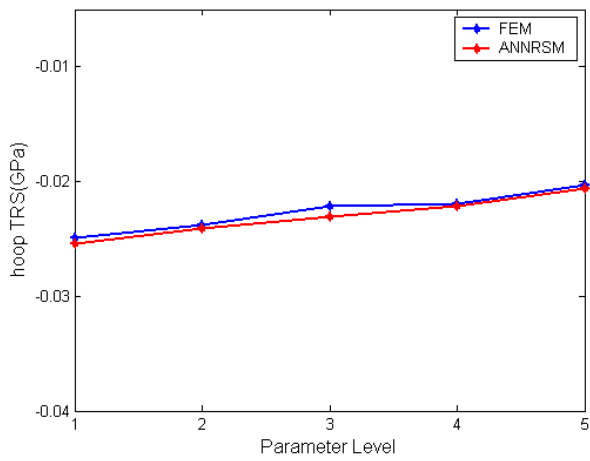
Fig. 13. Comparison of FEM's and ANNRSM's results with different level of d_4.

Fig. 14. Comparison of FEM's and ANNRSM's results with different level of d_5.
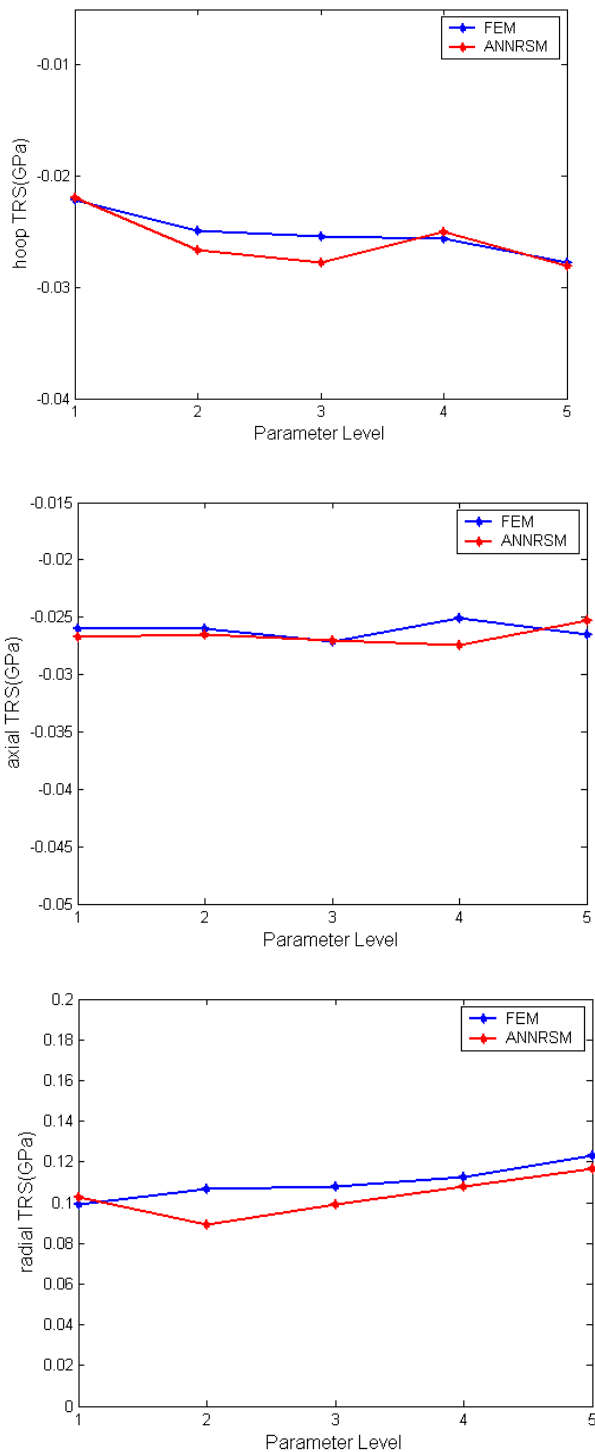
*Fig. 15. Comparison of FEM's and ANNRSM's results
with different level of d_6.*

5.3 Optimization results

The well-trained ANNRSM is used to find the minimum axial TRS, hoop TRS, radial RTS. The final optimized interphases thicknesses for minimum axial TRS are: $0.3\ \mu m$, $0.4\ \mu m$, $0.3\ \mu m$, $0.6\ \mu m$, $0.5\ \mu m$,

$0.3\ \mu m$. The final optimized interphases thicknesses for hoop TRS are: $0.6\ \mu m$, $0.3\ \mu m$, $0.5\ \mu m$, $0.4\ \mu m$, $0.5\ \mu m$, $0.3\ \mu m$. The final optimized interphases thicknesses for radial RTS are: $0.3\ \mu m$, $0.6\ \mu m$, $0.7\ \mu m$, $0.5\ \mu m$, $0.5\ \mu m$, $0.6\ \mu m$.

6. Conclusions

In this study, an integrated methodology based on finite element analysis, ANNRSM and DE algorithm is presented to approximate the functions between multi-layered interphases thicknesses and maximum TRS within CMCs. This integrated methodology can effectively find out the highly non-linear relationship between the design parameters and objective results and store this relationship in ANNRSM. The use of DE to train the ANNRSM proved to be an efficient technique. The results show the proposed methodology could estimate the TRS of different design solutions and identify the best one. The developed methodology in this paper can help evaluate the quality of design at the up-front of design stage and thus can greatly reduce the simulation time and make it possible to search for the optimal design in the whole design space.

References

[1] H. C. Cao, E. Bischo, O. Sbaizero, M. Ruhle, A. G. Evans, D. B. Marshall, J. J. Brennan, J. Am. Ceram. Soc. **73**, 1691 (1990).
[2] A. G. Evans, F. W. Zok, J. Davis, Compos. Sci. Technol. **42**, 3 (1991).
[3] G. Folsom, F. W. Zok, F. F. Lange, J. Am. Ceram. Soc. **77**, 2081 (1994).
[4] R. Naslain, Ceram. Trans. **58**, 23 (1995).
[5] C. Droillard, J. Lamon, X. Bourrat, Materials Research Society Symposium Proceedings **365**, 371 (1995).
[6] C. Droillard, J. Lamon, J. Am. Ceram. Soc. **79**, 849 (1996).
[7] J. L. Bobet, J. Lamon, Acta Metall. Mater. **43**, 2241 (1995).
[8] J. L. Bobet, J. Lamon, J. Alloy. Compd. **259**, 260 (1997).
[9] P. Vena, Meccanica **40**, 163 (2005).
[10] T. Noda, H. Araki, F. Abe, M. Okada, J. Nucl. Mater. **191-194**, 539 (1992).
[11] T. M. Besmann, J. C. McLaughlin, H. T. Lin, J. Nucl.

Mater. **219**, 31 (1995).

[12] A. H. Elhewy, E. Mesbahi, Y. Pu, Probabilist. Eng. Mech. **21**, 44 (2006).

[13] H. M. Gomes, A. M. Awruch, Struct. Safety. **26**, 49 (2004).

[14] L. Schueremans, D. Van Gemert, Struct. Safety. **27**, 246 (2005).

[15] F. X. Irisarri, D. H. Bassir, J. Maire, N. Carrere, Compos. Sci. Technol. **69**, 983 (2009).

[16] D. Bassir, S. Guessasma, L. Boubakar, Compos. Struct. **88**, 262 (2009).

[17] R. Storn, K. V. Price, J. Global Optim. **11**, 341 (1997).

[18] D. C. Ko, D. H. Kim, B. M. Kim, J. C. Choi, J. Mater. Process. Tech. **12**, 487 (1998).

[19] S. Guessasma, H. D. Bassir. Mech Adv Mater Struct. **16**, 293 (2009).

[20] S. Bertrand, C. Droillard, R. Pailler, X. Bourrat, R. Naslain, J. Eur. Ceram. Soc. **20**, 1 (2000).

[21] ANSYS 12.0 User's Manual, ANSYS Inc., Canonsburg, PA, USA.

_____

[*]Corresponding author: xu.yingjie@nwpu.edu.cn